Accepted Manuscript

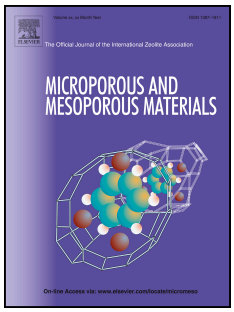

Influence of the synthesis conditions on the incorporation of B and the acidity in B-MCM-41 materials

Eliana G. Vaschetto, Gina A. Pecchi, Sandra G. Casuscelli, Griselda A. Eimer

PII: S1387-1811(16)30241-4

DOI: 10.1016/j.micromeso.2016.06.039

Reference: MICMAT 7781

To appear in: *Microporous and Mesoporous Materials*

Received Date: 2 May 2016

Revised Date: 27 June 2016

Accepted Date: 29 June 2016

Please cite this article as: E.G. Vaschetto, G.A. Pecchi, S.G. Casuscelli, G.A. Eimer, Influence of the synthesis conditions on the incorporation of B and the acidity in B-MCM-41 materials, *Microporous and Mesoporous Materials* (2016), doi: 10.1016/j.micromeso.2016.06.039.

Graphical Abstract

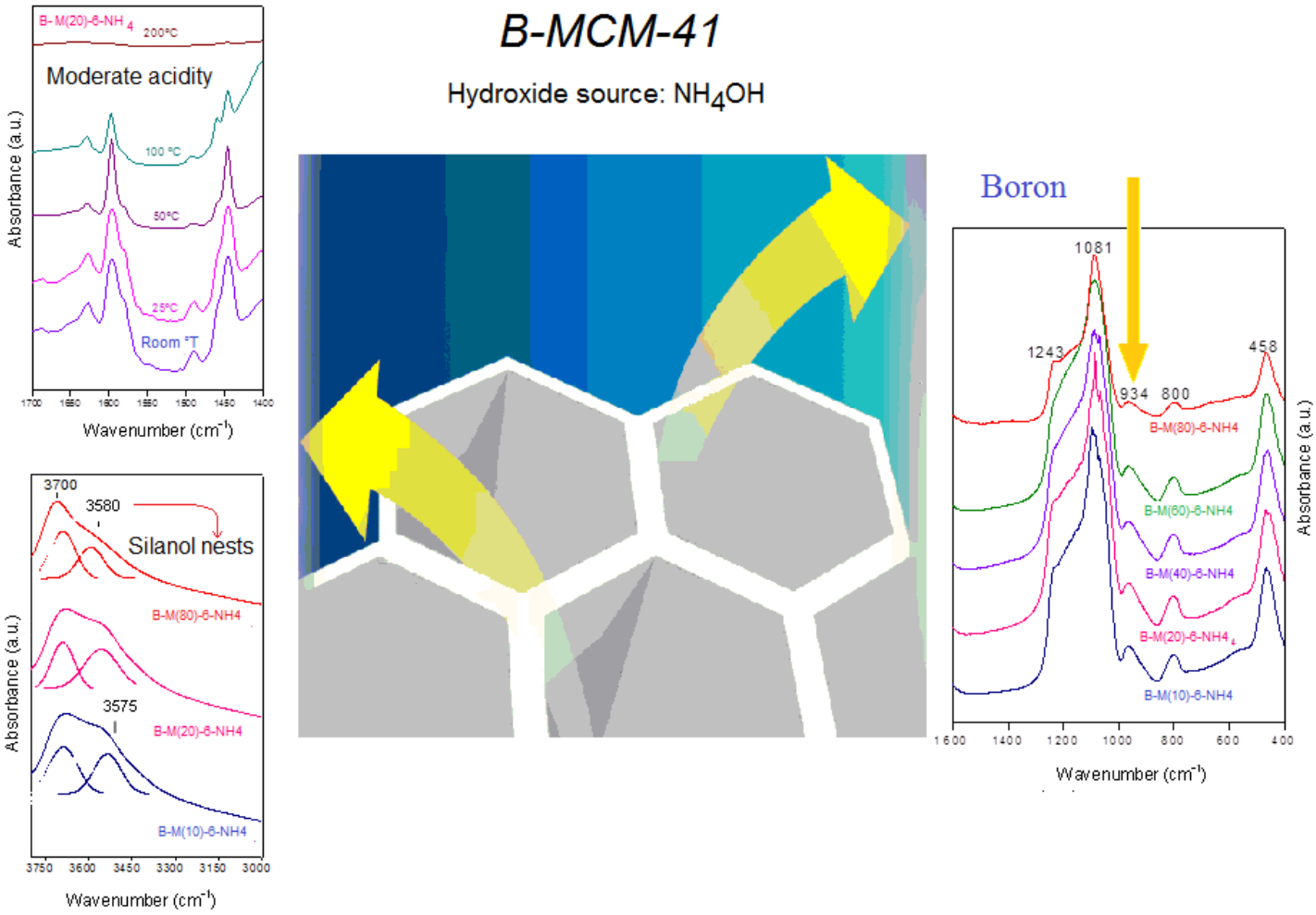

Influence of the synthesis conditions on the incorporation of B and the acidity in B-MCM-41 materials.

Eliana G. Vaschetto[a], Gina A. Pecchi[b], Sandra G. Casuscelli[a], Griselda A. Eimer[a].*

[a]Centro de Investigación y Tecnología Química (CITeQ, UTN, CONICET), Facultad Regional Córdoba, Maestro López y Cruz Roja Argentina, Ciudad Universitaria,CP: 5016 Córdoba, Argentina

[b]Facultad de Ciencias Químicas, Universidad de Concepción, Casilla160-C, Concepción, Chile

**e-mail: geimer@frc.utn.edu.ar ; griseeimer@yahoo.com.ar*

Abstract

B-MCM-41 type nano-structured materials were prepared by direct hydrothermal synthesis. The time of hydrothermal treatment, the Si/B initial molar ratio and the nature of the hydroxide source in the synthesis process were analyzed. All the materials were characterized by XRD, N_2 adsorption, TEM, SEM, ICP-OES, FT-IR and adsorption of pyridine coupled to FT-IR spectroscopy. The role of hydroxide source is essential to achieve the incorporation of boron in the mesoporous structure. The relationship between the Boron content in the synthesis gel, the degree of introduction of tetra-coordinated B into the framework, the formation of nest silanols and the relative density of the acidic sites have been discussed. We could corroborate that hydroxyl groups present in silanol nests are the direct responsible of the moderate Brønsted acidity of our materials. The enhancement in the density of acidic nest silanols was reached by increasing the B content in the mesoporous structure. Finally, the use of NH_4OH, as hydroxide source, Si/B initial molar ratio of 10 and 20 and a hydrothermal treatment of 6 days resulted the optimum synthesis conditions to obtain the highest framework B incorporation and more

abundant moderate Brønsted sites (silanol nests), thus improving the potencial catalytic properties of these materials.

Key words: Mesoporous Materials; B-MCM-41; silanol nests; moderate acidity.

1. Introduction

In recent years, MCM-41 mesoporous material appears as one of the most desirable candidates for different types of applications [1] like adsorption, molecular sieving and catalysis (being widely used as catalysts in reactions for the production of petrochemicals and fine chemicals). Other possible applications include the use as hosts for the formation of metal or semiconductor clusters, or for the controlled polymerization of conducting polymers in the form of molecular wires [2].

This mesoporous molecular sieve (a member of the M41S family), which possesses a hexagonally arranged uniform pore structure, was discovered by Beck et al. in 1992 [3]. Their most important characteristics are the large BET specific area, high porosity, controllable and narrowly distributed pore sizes. These characteristics manifest themselves as a very promising candidate as both catalyst support [4-6] and adsorbent [7-8]. Then, the isomorphous substitution of Si by a trivalent cation represents a way of reforming siliceous mesoporous materials because of the incorporation of acid sites. There is no doubt that the presence of large pores combined with acidic properties opens up new possibilities for processing and/or producing large molecules. Thus, the incorporation of foreign atoms in the framework of MCM-41 silica such as Al [9], Ga [10], Ti [11], V [12] and B [13-16] has already been reported.

Boron is widely distributed in the environment, from natural or anthropogenic sources [17]. It can be found mainly in the form of boric acid or borate salts. In the literature few reports are available on synthesis of B-MCM-41. However, the nature and strength of the acid sites have not been completely elucidated and more research is even necessary in this respect. In this paper, we develop and characterize B-MCM-41 catalysts. The synthesis conditions and hydroxide source were analized in relation to the structural properties and incorporation of

B into the framework. In the substitution of Si by B during the synthesis of MCM-41, we expected to modify the acidic properties of these materials and thereby their catalytic properties [18]. Therefore, the incorporation degree of the boron was correlated with the nature and strength of acid sites generated.

2. Experimental

2.1. Synthesis

The mesoporous materials (B-MCM-41) were prepared by hydrothermal synthesis using cetyltrimethylammonium bromide (CTABr, Merck, 99%) as template and tetraethoxysilane (TEOS, Aldrich, 98%) as silicon source. Sodium hydroxide (NaOH, Cicarelli) or ammonium hydroxide (NH_4OH, Cicarelli, 30%) aqueous solution 2 M was used for hydrolysis and pH adjustment, and boric acid (H_3BO_3, Cicarelli) was used as source of boron. The catalysts were synthesized from a synthesis gel of molar composition: NaOH/Si = 0.50, CTABr/Si = 0.12, H_2O/Si = 132 and Si/B = 10-80. In a typical synthesis, CTABr was dissolved in H_2O-NaOH or H_2O-NH_4OH solution and after heating (35-40 ℃) to dissolve the surfactant, the TEOS was added and stirred for 30 min. The B source was added and the synthesis gel was stirred at room temperature for 7h. Then, this resulting gel was hydrothermal treated at 100 ℃ in a Teflon-lined stainless-steel autoclave under autogeneous pressure for 0–8 days, (0 days corresponds to the material without hydrothermal treatment). The samples obtained were named as B-M(x)-y-z, where “x” is the Si/B initial molar ratio, “y” is the time of hydrothermal treatment and “z” refers to the source of hydroxide (Na=NaOH or NH_4=NH_4OH). For comparison, analogous boron-free MCM-41 samples were synthesized and named as Si-M-y-z.

The final solid was filtered, washed with distilled water and dried at 60 ℃ overnight. To remove the template, the samples were heated (heating rate of 2 ℃/min) under N_2 flow up to 500 ℃ and kept at this temperature for 6 h; they were then calcined at 500 ℃ under air flow for 6 h .

2.2. Characterization

The X-ray diffraction (XRD) patterns were recorded in air at room temperature on a Philips PW 3830 diffractometer with Cu Kα radiation (λ= 1.5418 Å) in the range of 2θ from 1.5° to 7°. Specific surfaces were measured u sing a Pulse Chemisorb equipment by single point at P/P_0 = 0.3 through the BET method. The samples were previously heated for 1 h at 300 °C under N_2 flow.

The Boron content was determined by inductively coupled plasma optical emission spectroscopy (ICP-OES), using a VISTA-MPC CCD Simultaneos ICP-OES-VARIAN.

Infrared analysis of the samples was recorded on a JASCO 5300 FT-IR spectrometer. The FT-IR spectra in the lattice vibration region were performed using the KBr 0.05% wafer technique. In addition, in order to evaluate the strength and type of acid sites, FT-IR spectral measurements of pyridine adsorbed on the samples were also performed through the following procedure: Self-supported wafers of the samples (~20 mg and 13 mm of diameter) were prepared, placed in a thermostatized cell with CaF_2 windows connected to a vacuum line and evacuated for 7 h at 400 ℃ under a dynamic vacuum; residual pressure was smaller than 10-3 Pa. After cooling to room temperature, the spectrum of each sample was recorded (background spectrum). Afterwards the background spectrum was recorded, the solid wafer was exposed to pyridine vapors (Sintorgan, 99% purity) until saturate the system to 46 mm Hg at room temperature; the contact time at this pressure was 12 h. After an IR spectrum of the adsorbed pyridine at room temperature was recorded, the subsequent IR spectra were obtained following the pyridine desorption by evacuation for 1 h at 25, 50, 100 and 200 ℃. Finally, the difference spe ctrum for each sample was obtained by subtracting the background recorded previously.

3. Results and discussion

3.1 Mesoporous materials synthesized using NaOH

Table 1 summarizes the different synthesis conditions and physicochemical properties for the samples prepared in this study using NaOH. Figure 1 shows the XRD patterns of the samples with initial Si/B molar ratios = 20 and 60, obtained by stirring the reaction mixture for 7 h followed by different times of

hydrothermal treatment (0-8 days). All of the patterns exhibit a main (100) peak and two weak reflections ascribed to (110) and (200) diffraction planes, which is typical of highly ordered MCM-41 structures and consistent with the high surface values obtained (above 880 m^2/g). As it can be observed in both cases (Si/B ratios = 20 and 60), even though the mesostructure was formed without thermal treatment, a notable improvement of the original structure was achieved when the samples were hydrothermal treated for 6 h. Then, a longer time seems to induce some disorder in the structure which can be also correlated with a decrease in the surface observed (Table 1).

Figure 2 shows the FT-IR spectra in the range 1400-400 cm^{-1} for the samples B-M(20)-6-Na and B-M(60)-6-Na, compared to pure siliceous material. As it can be seen these samples showed, besides the peaks characteristic of the Si-O bond vibrations (1243, 1081, 800 and 458 cm^{-1}) [19-22], a band clearly visible at 960 cm^{-1} which can be interpreted in terms of the overlapping of both Si–OH and Si–O–B bonds vibrations. Even if this signal for B-M samples may be attributed to the incorporation of a heteroatom in the structure [22-24], no significant differences with that of pure silica suggest the absence of boron incorporated into the network. This fact was corroborated by ICP; thus the presence of B in the solids was not detected by this technique (Table 1).

In order to detect the presence of silanol groups on the surface, Figure 3A depicts the FT-IR spectra in the hydroxyl range of the B-M(20)-6-Na, B-M(60)-6-Na samples and of the purely siliceous analog. Before measurements, self-supported wafers of the samples were degassed at 400 ℃ for 7 h. It is known that there can be several types of surface silanol groups with different acidic properties: terminal, geminal, vicinal and nests [25-29]. All our spectra exhibited a broad and intense band, attributed to hydrogen bonded to hydroxyl groups [26,28], that could be deconvoluted into two contributions at about 3700 and 3590 cm^{-1}. According to the literature [25-27] these two contributions have been assigned respectively to hydrogen bonded to terminal/vicinal silanol groups and silanol nests generated at framework defect sites. It is known that the introduction of a heteroatom inside the framework, substituting to Si, can generate such structural defect sites. However, the integrated absorbance of the 3590 cm^{-1} band similar in the three materials would be indicating the lack of

additional nest silanols with respect to the siliceous material, and consequently that the boron could not be incorporated into the framework (Fig. 3A).

The chemisorption of pyridine followed by IR studies is usually a useful probe to detect the presence and nature of acid sites on a catalyst [30-33]. Fig. 3(B) shows the FT-IR spectra of adsorbed pyridine at room temperature on the B-M(20)-6-Na, B-M(60)-6-Na samples and the purely siliceous analog. The samples show bands at 1597 and 1447 cm^{-1} assigned to pyridine bonded to silanol groups whose hydroxyls are not capable to protonate pyridine [28, 30-37]. However, these bands can also present a contribution arising from pyridine bonded to Lewis acid sites. On the other hand, the presence of a band at 1632 cm^{-1}, has been attributed by us to pyridine interacting with acid hydroxyls (Brønsted sites) [29, 38, 39], such as the nest silanols associated with the 3600-3590 cm^{-1} band. Even if we have found that these acid sites are of a very weak character [40] Sato and co-workers [25] have reported that the nest silanol's acidity is the strongest of all the different silanol species [25,27]. With attention to the signal at 1632 cm^{-1} [41-43], no significant differences were observed for the different samples, concluding that the three samples have characteristics similar to pure siliceous material.

The cause of the formation of these purely siliceous materials (without heteroatom incorporation), is probably due to the use of a strong base "*sodium hydroxide*" in conjunction with a weak acid "*boric acid*" as source of Boron. This leads to a favored neutralization reaction at the start of synthesis, with the formation of sodium borate (Na_3BO_3). This compound exhibits high water solubility and therefore, the Na_3BO_3 solution would be completely removed in the washing and filtering steps, without achieving the incorporation of heteroatom in the structure.

$$H_3BO_3 + 3\,NaOH \rightarrow Na_3BO_3 + 3\,H_2O$$

Taking into account the mentioned above, if in contrast, a weak base (NH_4OH whose Kb = $1.8 * 10^{-5}$) is used, the neutralization reaction of H_3BO_3 during the synthesis process will not happen in the same degree that when NaOH is used. Thus, the boric acid would remain in the synthesis medium for that the boron can interact with the silicon species and be incorporated in the mesoporous

network. In view of this, the hydroxide source was changed by "*ammonium hydroxide" and the synthesis were again carried out via hydrothermal treatment* during 6 days. The boron content in the initial gel was varied between Si/B molar ratios 10 and 80.

3.2 Mesoporous materials synthesized using NH_4OH.

According to the XRD patterns shown in Figure 4, using NH_4OH as hydroxide source, mesoporous structures with characteristic peaks corresponding to the (100), (110) and (200) planes, were also obtained. In addition, with increasing boron content, the structural regularity was favored which is consistent with the increased values of specific areas (Table 2).

Then, the N_2 physisorption was carried out in order to complete the information about the structure of the samples. The average pore diameter (Dp), calculated by the BJH method, was around of 4.14 nm for all the samples. In addition, the samples showed high specific surface (~ 800 m^2/g) and pore volumen (Vp ~ 0.75 cm^3/g), typical of mesoporous materials. These high values are according with the good structural order observed by XRD.

Measurements of transmission electron microscopy of the materials were made in order to corroborate their structural regularity. TEM images of representative samples are shown in Figure 5. The materials presented a well-defined mesoporous structure, exhibiting well-ordered parallel straight mesochannels characteristic of the hexagonal pore arrangement of MCM-41 type materials [43, 44], which was already inferred by us in the XRD patterns. It should be noted that in Fig. 5(C) the image is viewed perpendicularly to the direction of the pore arrangement [45], clearly showing the presence of straight mesochannels arraying along the long axis [46]; meanwhile, the hexagonal arrangement of the unidirectional mesopores is clear in Fig. 5(A) and (B) where a frontal view of them can be observed.

SEM images of some samples taken as representative are shown in Figure 6. These images indicate the presence of particles that do not display any particular crystalline habit or morphology, although the spherical-like morphology seems to be the dominant one. The primary particles are very small and appear to be aggregated into larger secondary particles which exist in

various sizes. These apparently single particles observed in the SEM could be the result of intergrowth of multiple smaller particles [47].

The infrared spectra in the 1600-400 cm^{-1} range for all the samples synthetized using NH_4OH and different B contents are shown in Figure 7. Besides the main bands described in the literature for MCM-41. A band at 934 cm^{-1}, interpreted in terms of the overlapping of both Si-O-H and Si-O-B bond vibrations, is clearly visible. The increase in the integrated absorbance of this band (A_{934}), when the B content increases (observed in Fig. 7), can be considered a proof of the tetra-coordinated boron incorporation, replacing to Si into the framework [48-51]. Then, as it is shown in Table 2, the presence of B in these solids (wt.%) could be detected by ICP spectroscopy. Table 2 also summarizes the mentionated A_{934} values.

Figure 8 depicts the FT-IR spectra of the samples more representative in the hydroxyl range. The spectra show a broad and intense band that is deconvoluted into two contributions at about 3700 and 3580 cm^{-1}. Taking into account the origin of both contributions (explained above) and comparing the integrated absorbances of the same, it is possible to observe that the relative proportion of silanol nests increases for the samples with higher B contents which, at the same time, exhibit the higher framework boron amount (see Table 2 and Fig. 8). This fact would indicate that increasing the boron amount inside the framework, the formation of structural defects [28] is increased leading to a higher proportion of silanol nests.

The figure 9A shows the FT-IR spectra recorded after the adsorption of pyridine at room temperature and subsequent evacuation at 25, 50, 100 and 200 ℃ for the B-M(20)NH_4 material. All the samples show the bands at 1597, 1447 and 1632 cm^{-1}, already previously assigned. Moreover, a shoulder at 1450 cm^{-1} appears more defined under evacuation at higher temperatures giving account for the contribution arising from pyridine bonded to Lewis acid sites. Then, under evacuation at 200 ℃ all of the bands tend to disappear, indicating the moderate character of the acidity of these samples.

Figure 9B shows FT-IR of pyridine adsorbed at room temperature on samples synthesized with different Si/B molar ratios. Taking into account that all of the measurements were affected by the wafer weight, the integrated absorbances of the 1632 cm^{-1} IR band (A_{1632}) (arising from acid silanols) after pyridine

absorption at room temperature, have been calculated to estimate the Brønsted sites relative density (Table 2). An increase in the acid silanols density can be clearly associated with the higher proportion of framework B, according to the boron content increasing. Thus, the results confirm that the introduction of B into the mesoporous framework increases the proportion of silanol nests, which present Brønsted acidity likely due to an inductive effect originated by the heteroatom presence (Fig. 9B and Table 2).

In order to shed light on the origin of the Brønsted acidity in these materials, A_{1632} (associated with the Brønsted sites relative density) has been graphed vs. A_{934} (as indicative of the B incorporation into framework) and vs. A_{3590} (associated to nest silanols proportion) (Figure 10). It is observed in Fig. 10-curve "b" that while initially the acid sites density associated to the hydroxyls (A_{1632}) is slowly increased with the framework B content increasing, the same is very strongly increased for the samples with higher B incorporation inside the structure (above A_{934} = 0.38). Likewise, it is very clear the linear increase in the acid hydroxyls density when the proportion of nest silanols (A_{3590}) increases (curve "a" in Fig. 10). Therefore, these observations confirm that the acidity of our samples arising from hydroxyl groups (silanols) is due to the silanol nests. These species would be mainly generated from the introduction of B inside the framework and their acid properties would be caused by an inductive effect of the heteroatom present. Thus, changes in the electron density around Si due to charge unbalance, or differences in electronegativity or local structure deformation resulting from the B incorporation may weaken the Si-O-H bond in the silanol nests giving them the acid properties. Then, above a critical proportion of framework B, the formation of these structural defects would be quickly increased, leading to a proportion of nest silanols (responsible of the observed acidity) strongly increasing with the framework B amount.

4. Conclusion

B-MCM-41 molecular sieves have been successfully prepared by a direct synthesis method. The influence of various synthesis conditions such as metal content, source of hydroxide and times of hydrothermal treatment on the acid

and structural properties has been systematically investigated. The hexagonal pore arrangement typical of MCM-41 materials was clearly visualized by TEM and inferred by XRD.

The employed synthesis procedure when NH_4OH was used as hydroxide source leaded to the incorporation of B in tetrahedral coordination into the framework and the formation of silanol nests at framework defect sites, which increase with the B content increasing. Studies of adsorption and thermodesorption of pyridine followed by FT-IR allowed us to identify a moderate Brønsted acidity from hydroxyl groups present in our B-MCM-41 samples which could be clearly associated with the nest silanols.

Thus, a linear relationship between the Brønsted sites density and the proportion of silanol nests was found. Therefore, by varying the B content in the synthesis gel, using NH_4OH as hydroxide source and 6 days of hydrothermal treatment, we have achieved an increase in the density of nest silanols in this type of mesoporous silicates, thus improving their potencial catalytic properties by incorporating moderate acidity sites.

5. Acknowledgements

This work was supported by the CONICET and UTN-FRC of Argentina. We gratefully acknowledge the support from MINCYT of Argentina and CONICYT from Chile through the project Cód CH/12/03. The authors are grateful to Geol. Julio Fernandez for the IR spectra.

6. References

[1] Q. Qi, T. Zhang, X. Zheng, L. Wan, Sensors Actuators B 135 (2008) 255–261.

[2] C.-G. Wu and T. Bein. Zeolites and Related Microporous Materials. 84 (1994) 2269-2279.

[3] J.S. Beck, J.C. Vartuli, J.W. Roth, M.E. Leonowicz, C.T. Kresege, K.D. Schmitt, C.T.-W. Chu, D.H. Olsen, E.W. Sheppard, S.C. McCullen, J.B. Higgins, J.L. Schlenker, J.Am. Chem. Soc. 114 (1992) 10834–10843.

[4] R.K. Kloetstra, H. van Bekkum, J. Chem. Res. (Symp.) (1995) 26–27.

[5] A. Corma, A. Martínez, V. Martínez-Soria, J.B. Montón, J. Catal. 153 (1995) 25–31.

[6] A. Sayari, Chem. Mater. 8 (1996) 1840–1852.

[7] P.J. Branton, P.G. Hall, K.S.W. Sing, J. Chem. Soc., Chem. Commun. (1993) 1257–1258.

[8] J. Rathousky, A. Zukai, O. Franke, G. Schulz-Ekloff, J. Chem. Soc. 90 (1994) 2821–2826.

[9] K.M. Reddy, C.S. Song, Catal. Lett. 36 (1996) 103–109.

[10] T. Blasco, A. Corma, M.T. Navarro, J.P. Pariente, J. Catal. 156 (1995) 65–74.

[11] Z. Gabelica, J.M. Clacens, R. Sobry, G.V. VandeBrossche, Stud. Surf. Sci. Catal. 97 (1995) 143–147.

[12] K.M. Reddy, I.L. Moudrakovski, A. Sayari, J. Chem. Soc. Chem. Commun. (1994) 1059–1060.

[13] D. Trong On, P.N. Joshi, J. Lemay, S. Kaliaguine, Surf. Sci. Catal. 97 (1995) 543–549.

[14] A. Sayari, C. Danumah, I.L. Moudrakovski, Chem. Mater. 7 (1995) 813–815.

[15] A. Chenite, Y. Le Page, A. Sayari, Chem. Mater. 7 (1995) 1015–1019.

[16] U. Oberhagemann, I. Topalovic, B. Marler, H. Gies, Stud. Surf. Sci. Catal. 98 (1995) 17–18

[17] Oznur Kaftan, Muge Acıkel, Ahmet E. Eroglu, Talal Shahwan, Levent Artok, Chaoying Ni. Analytica Chimica Acta 547 (2005) 31–41.

[18] M.R. Klotz, US Patents 4 268 420; 4 269 813; 4 285 919 (1981).

[19] G. Eimer, L. Pierella, G. Monti, O. Anunziata, Catal. Lett. 78 (2002) 65-75.

[20] G. Eimer, L. Pierella, G. Monti, O. Anunziata, Catal. Commun. 4 (2003) 118-123.

[21] G. Eimer, S. Casuscelli, G. Ghione, M. Crivello, E. Herrero, Appl. Catal. A 298 (2006) 232-242.

[22] A. Palani, N. Gokulakrishnan, M. Palanichamy, A. Pandurangan, Appl. Catal. A 304 (2006) 152-158.

[23] A. Corma, Chem. Rev. 97 (1997) 2373-2420.

[24] M. Selvaraj, A. Pandurangan, K.S. Seshadri, P.K. Sinha, K.B. Lal, Appl. Catal. A 242 (2003) 264-274.

[25] Y. Izumi, H. Ichihashi, Y. Shimazu, M. Kitamura, H. Sato, Bull. Chem. Soc. Jpn. 80 (7) (2007) 1280‑1287.

[26] W.F. Holderich, J. Roseler, G. Heitmann, A.T. Liebens, Catal. Today 37 (1997) 353‑366.

[27] H. Ichihashi, Sci. Technol. 145 (2002) 73‑84.

[28] A. Jentys, K. Kleestorfer, H. Vinek, Micropor. Mesopor. Mater. 27 (1999) 321‑328.

[29] V.L. Zholobenko, D. Plant, A.J. Evans, S. Holmes, Micropor. Mesopor. Mater. 44 (2001) 793‑799.

[30] C.M. Chanquiía, L. Andrini, J.D. Fernández, M.E. Crivello, F.G. Requejo, E.R. Herrero, G.A. Eimer, J. Phys. Chem. C 114 (2010) 12221–12229.

[31] B. Chakraborty, B. Viswanathan, Catal. Today 49 (1999) 253–260.

[32] M. Hunger, U. Schenk, M. Breuninger, R. Gläser, J. Weitkamp, Micropor. Mesopor. Mater. 27 (1999) 261–271.

[33] X.S. Zhao, G.Q. Lu, A.K. Whittaker, G.J. Millar, H.Y. Zhu, J. Phys. Chem. B 101 (1997) 6525–6531.

[34] T.D. Conesa, J.M. Hidalgo, R. Luque, J.M. Campelo, A.A. Romero, Appl. Catal. A 299 (2006) 224–234.

[35] G.A. Eimer, S.G. Casuscelli, C.M. Chanquia, V.R. Elías, M.E. Crivello, E.R. Herrero, Catal. Today 133 (2008) 639–646.

[36] D. Trong On, S.V. Nguyen, V. Hulea, E. Dumitriu, S. Kaliaguine, Micropor. Mespor. Mater. 57 (2003) 169–180.

[37] D. Srinivas, R. Srivastava, P. Ratnasamy, Catal. Today 96 (2004) 127–133.

[38] C. Otero Arean, M. Rodriguez Delgado, V. Montouillout, J.C. Lavalley, C. Fernandez, J.J. Cuart Pascual, J.B. Parra, Micropor. Mesopor. Mater. 67 (2004) 259–264.

[39] E. Escalona Platero, M. Peñarroya Mentruit, C. Otero Areán, A. Zecchina, J. Catal. 162 (1996) 268–276.

[40] E.G. Vaschetto, G.A. Monti, E.R. Herrero, S.G. Casuscelli, G.A. Eimer, Appl. Catal. A 453 (2013) 391–402.

[41] T. Yashima, K. Miura, T. Komatsu, Stud. Surf. Sci. Catal. 84 (1994) 1897–1904.

[42] P. O'Sullivan, L. Forni, B.K. Hadnett, Ind. Eng. Chem. Res. 40 (2001) 1471–1475.

[43] S. Rodrigues, S. Uma, I. Martyanov, K.J. Klabunde, J. Photochem. Photobiol. A 1–3 (165) (2004) 51–58.

[44] V.R. Elías, E.V. Sabre, K. Sapag, S.G. Casuscelli, G.A. Eimer, Appl. Catal. A 413–414 (2012) 280–291.

[45] K. Choi, R. Wakabayashi, T. Tatsumi, T. Yokoi, K. Kuroda, J. Colloid Interface Sci. 359 (2011) 240–247.

[46] Y. Xu, G. Zhou, C. Wu, T. Li, H. Song, Solid State Sci. 13 (2011) 867–874.

[47] M.A. Betiha, S.A. Mahmoud, M.F. Menoufy, A.M. Al-Sabagh, Appl. Catal. B 3–4 (107) (2011) 316–326.

[48] A.U.B. Queiroz, L.T. Aikawa, French Patent 2694000, 1994.

[49] I. Eswaramoorthi, A.K. Dalai, Microporous Mesoporous Mater. 93 (2006) 1-11.

[50] Mehdi Adjdir, Tewfik Ali-Dahmane, Peter G. Weidler. C. R. Chimie 12 (2009) 793-800.

[51] Paper 4] D. Trong On, P.N. Joshi, G. Lemay and S. Kaliaguine. Zeolites: A Refined Tool for Designing Catalytic Sites (1995) 543-549.

Figure captions:

Figure 1: XRD patterns of samples synthesized with NaOH at different hydrothermal treatment times and Si/B molar ratios: **(A)** 20 and **(B)** 60.

Figure 2: FT-IR spectra in the 400–1600 cm^{-1} range of Si-M-6-Na, B-M(20)-6-Na and B-M(60)-6-Na samples, synthesized by hydrothermal treatment during 6 days.

Figure 3: FT-IR spectra of the Si-M-6-Na, B-M(20)-6-Na and B-M(60)-6-Na catalysts: **(A)** in the hydroxyl stretching region after degassing at 400 ℃; **(B)** of pyridine adsorbed at room temperatura in the 1700-1400 cm^{-1} region.

Figure 4: XRD patterns of samples synthesized with NH_4OH at hydrothermal treatment during 6 days and different Si/B molar ratios.

Figure 5: Transmission electron microscopy images: **(A)** B-M(20)-6-NH_4, **(B)** B-M(10)-6-NH_4 and **(C)** B-M(60)-6-NH_4.

Figure 6: Scanning electron micrographs of: **(A)** B-M(20)-6-NH_4, **(B)** B-M(60)-6-NH_4 and **(C)** B-M(10)-6-NH_4.

Figure 7: FT-IR spectra in the 400–1600 cm^{-1} range of the samples synthesized with NH_4OH, hydrothermal treatment during 6 days and different Si/B molar ratios.

Figure 8: FT-IR spectra in the hydroxyl stretching region after degassing at 400 ℃ for B-M(80)-6-NH_4, B-M(20)-6-NH_4 and B-M(10)-6-NH_4.

Figure 9: (A) FT-IR of pyridine adsorbed on the B-M(20)-6-NH_4 sample at room temperature and after subsequent evacuation at 25, 50, 100 and 200 ℃; **(B)** FT-IR of pyridine adsorbed at room temperature on samples synthesized with different Si/B molar ratios.

Figure 10: A_{1632} vs. (a) A_{3590} and (b) A_{934}.

Table 1: Physicochemical properties of solids synthesized with NaOH and different hydrothermal treatment times for samples with: Si/B molar ratios of 20 and 60 and for the purely siliceous analog.

Table 1

Sample	Si/B[(a)]	Hydrothermal treatment (days)	Area (m^2/g)	B content (wt.%)[(b)]
B-M(20)-0-Na	20	0	1023	N. D.
B-M(20)-1- Na	20	1	1105	N. D.
B-M(20)-6- Na	20	6	1215	N. D.
B-M(20)-8-Na	20	8	891	N. D.
B-M(60)-0-Na	60	0	992	N. D.
B-M(60)-1-Na	60	1	1048	N. D.
B-M(60)-6-Na	60	6	1220	N. D.
B-M(60)-8-Na	60	8	889	N. D.
Si-M-6-Na	-	6	1182	-

[a] Si/B initial molar ratio in the synthesis gel.
[b] By ICP-OES.
N.D.: Not Detected

Table 2: Physicochemical properties and infrared data for the solids synthesized with NH_4OH, hydrothermal treatment during 6 days and different Si/B molar ratios.

Sample	Si/B[(a)]	Si/B[(b)]	Area (m^2/g)	B content (wt%)[(c)]	A_{934}	A_{1632}
B-M(10)-6-NH_4	10	15.1	825	1.54	0.59	0.25
B-M(20)-6-NH_4	20	15.7	819	1.49	0.57	0.21
B-M(40)-6-NH_4	40	27.3	815	0.86	0.49	0.15
B-M(60)-6-NH_4	60	35.1	805	0.67	0.39	0.09
B-M(80)-6-NH_4	80	82.0	791	0.29	0.21	0.06

[a] Si/B initial molar ratio in the synthesis gel.
[b] Si/B final molar ratio in the synthesis gel.
[c] By ICP-OES.

Figure 1:

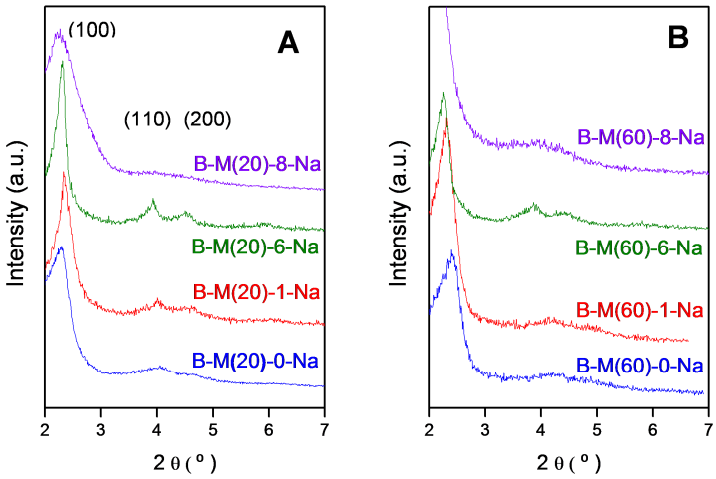

Figure 2

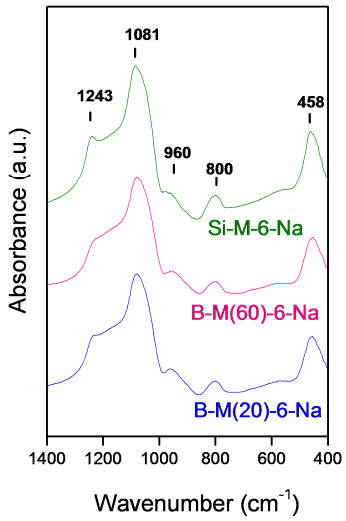

Figure 3

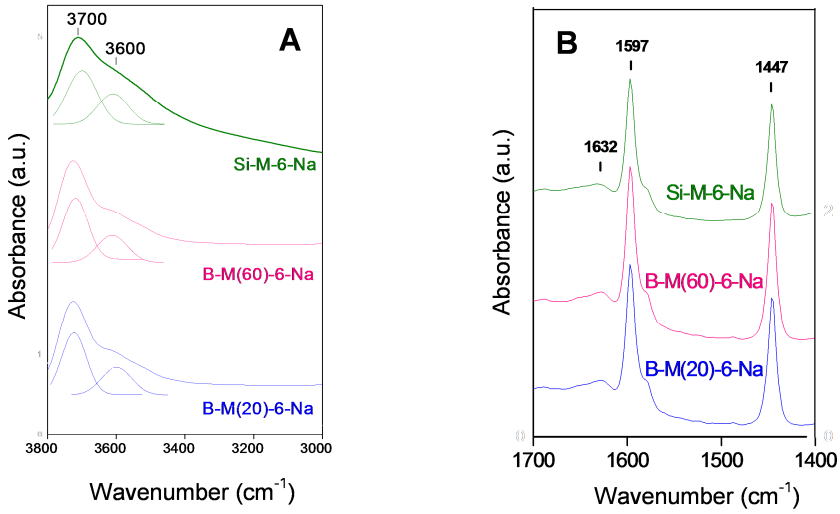

Figure 4

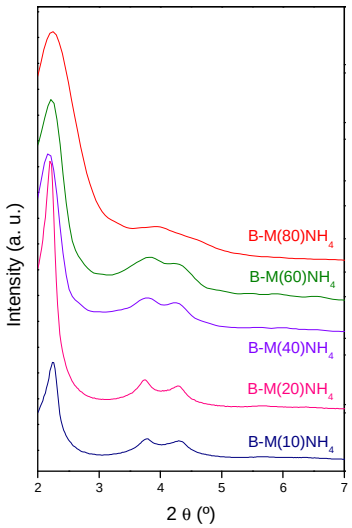

Figure 5

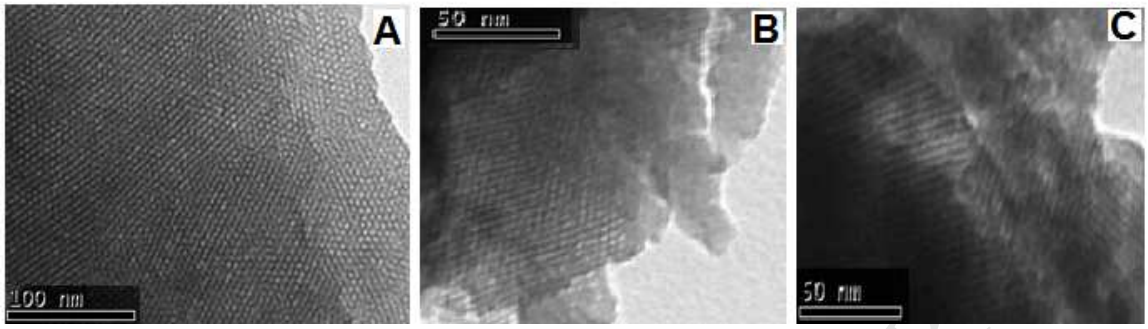

Figure 6

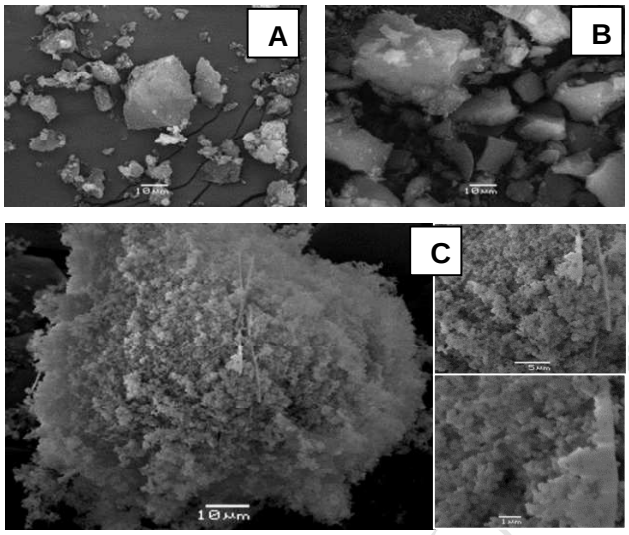

Figure 7

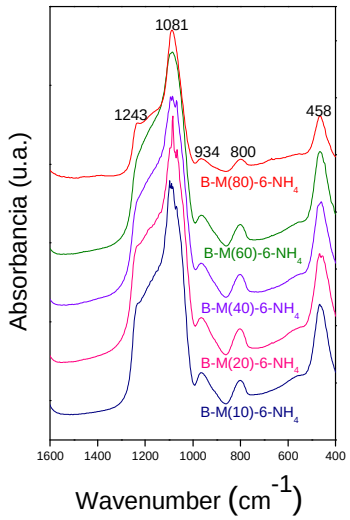

Figure 8

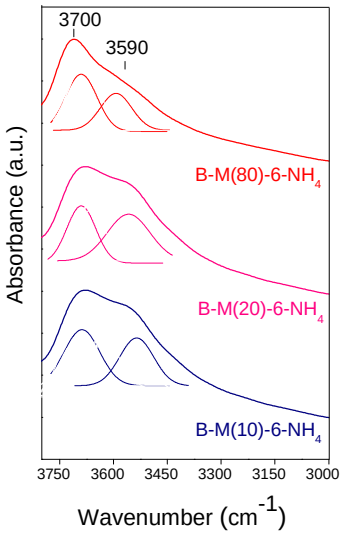

Figure 9

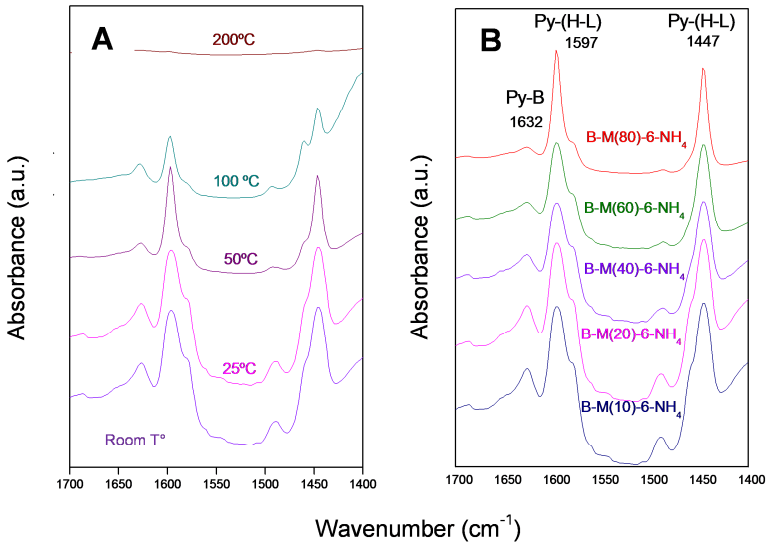

Figure 10

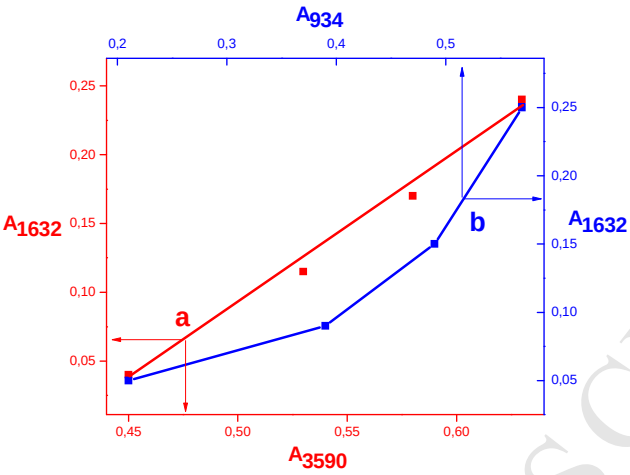

Highlights

- Nano-structured B-MCM-41 has been prepared with different B contents.
- Boron could be tetraedrally incorporated into framework using NH4OH as hydroxide source.
- The incorporation of boron leads to the formation of silanol nests.
- The moderate acid character present in samples is purely caused by the nest silanols.
- The potencial catalytic properties can be achieved by incorporating moderate acidity sites.